Surface Tension Effect on Transmembrane Channel Stability in a Model Membrane

Qing Zhu and Mark W. Vaughn*

Department of Chemical Engineering, P.O. Box 43121, Texas Tech University, Lubbock, Texas 79409-3121

Received: March 17, 2005; In Final Form: July 15, 2005

The effect of surface tension on the lipid bilayer membrane is a question that has drawn considerable research effort. This interest has been driven both by the desire to determine the surface tension effects on the lipid bilayer and from the suggestion that adding finite surface tension to a small membrane system may provide more realistic lipid properties in molecular dynamics simulations. Here, the effect of surface tension on a palmitololelylphosphatidylcholine (POPC) bilayer membrane containing a four-helix transmembrane alamethicin peptide bundle is investigated. Simulations of 10 ns were undertaken for two different ensembles, NPT and $NP_z\gamma T$ with a surface tension, γ, of 20 mN m^{-1} per interface, which is near the pore-forming region. The significance of differences between the tension-free and surface tension simulations was determined using nonparametric statistical analysis on replicate simulations with different initial conditions. The results suggest that, when the membrane is under surface tension, the peptide helical structure is perturbed from that in the tension-free state but that the bundle conformation is more stable than that in the tension-free state, with hydrogen bonding playing an important stabilizing role. Surface tension counteracts the influence of the transmembrane helix bundle on nearby lipid order, making the lipid order more uniform throughout the membrane in the tension state. Conversely, the lipid mobility was less uniform in the tension state, with lipids far from the bundle being significantly more mobile than those near the bundle. One general implication of the results is that surface tension can affect the membrane nonuniformly, in that the properties of lipids near the peptide are different from those further away.

1. Introduction

Much progress in understanding the structure of the lipid membrane has been made in the last 25 years, and the "fluid mosaic" model[1] has been refined to account for the mutual interactions of lipids and membrane associated proteins. Membrane embedded proteins have a crucial influence on membrane function, and protein activity can be affected by membrane stresses.[2] Many cells are exposed to stress from mechanical deformation and fluid frictional forces, and these forces have considerable effects,[3] some of which may be mediated by the membrane associated proteins. Although in vivo flow and mechanical induced stresses are anisotropic, surface tension may provide a first approximation to their effect on the membrane.

The effect of an applied surface tension on the lipid bilayer has been a long-term topic of interest for membrane simulations, and it is currently an area of active research. Many of these studies have focused on the application of surface tension to make membrane properties, such as lipid area per headgroup, match experiment;[4−6] however, some recent investigations have addressed the biophysical effects of surface tension such as its effect on undulations[7] or pore formation.[8]

It has been suggested that, in phospholipid membrane simulations, surface tension should be applied to counteract the small-system effect of the simulation cell and to give a more realistic result for the surface area per lipid.[4,9] As an example, Sankararamakrishnan and Weinstein[10] found that a pure dimyristoyl phosphatidylcholine (DMPC) system of 90 lipids simulated using CHARMM[11] and the particle mesh Ewald (PME) algorithm[12] for long-range electrostatics required an applied surface tension of 25−30 mN m^{-1} per interface to maintain a realistic area per lipid.

Others, however, argue that zero surface tension is the appropriate state for an unstressed bilayer at its free energy minimum and therefore an isotropic pressure is correct for molecular dynamics (MD) bilayer simulations.[13,14] Similarly, it has been suggested that improved force fields[7] and careful choice of the methodology[15] could eliminate the system-size effect without imposing a surface tension. For instance, area per lipid is particularly sensitive to the treatment of long-range electrostatics.[15]

It should be noted that many biological and pharmacological membranes are normally exposed to surface stress, so there may be external sources of membrane tension. Examples include cells exposed to blood flow or mechanical deformation, liposomes undergoing extrusion or processing, or hypotonic systems. Furthermore, size-dependent phenomena, such as surface undulations,[4,7] do exist, so it is not unexpected that finite size effects could be present, although for some model bilayer systems they may be negligible.[7] Therefore, there are some systems for which a nonzero surface tension is physical.

Aside from methodological considerations such as PME versus cutoff, area per lipid can vary significantly with the choice of force field, even under similar simulation conditions. Dynamic properties such as lipid mobility and lipid tail order are strongly affected by the area per lipid, so realistic values of this parameter are important. Imposing a surface tension is a common method to ensure the simulation values of lipid area match experimental measurements. A number of force fields are in common use. Surface tension ($NP_z\gamma T$) or fixed area

* Corresponding author. Phone: (806) 742-0451. Fax: (806) 742−3552. E-mail: mark.vaughn@ttu.edu.

10.1021/jp051419k CCC: $30.25
Published on Web 09/28/2005

(NP_zAT) ensembles are generally used with CHARMM[10,16−18] or GROMOS;[19,20] these force fields typically underestimate experimental values for the area per lipid of stress-free membranes. Typically, a surface tension of 10−35 mN m^{-1} per membrane leaflet was used. The NPT ensemble is often used for simulations using OPLS,[21,22] modified OPLS and GROMOS,[15,23,24] and GROMACS,[7,25] since these force fields usually give estimates for area per lipid of stress-free systems near (or slightly above) experimental values.

Separate from the issue of membrane tension, a physiologically and theoretically important question is how lipid membranes interact with embedded protein. Membrane proteins often contain bundles of transmembrane helices, so they are often represented by parallel α-helices forming ion channels. A simple model of these channels is provided by the transmembrane helix bundles of antimicrobial peptides, which transfer ions and water molecules through the lipid bilayer.[26] One of the most widely studied channel-forming peptides in both experimental and computational work is the 20-residue antibacterial peptide alamethicin.[23,27−32]

In what follows, we investigate the interaction of palmitololelylphosphatidylcholine (POPC) lipid with a small transmembrane channel of four alamethicin peptides[31] in a tense membrane. When the lipid bilayer contains an integral membrane protein, both the protein and the membrane will be perturbed from their pure state, and the behavior and properties of the adjacent lipid molecules are affected.[18,33] We are interested in these interactions when the applied surface tension is near that required to rupture the membrane. Our primary purpose is to investigate the effect of lipid/peptide interactions on membrane properties and protein/membrane stability. We use the GROMACS force field and assume that the applied surface tension will thermodynamically stretch the membrane beyond its equilibrium state.

Our secondary purpose is to deduce the general behavior of lipid/protein interactions that may be applicable whenever surface tension is applied, whether it be to provide the proper area per headgroup or to investigate phenomena that involved a stressed membrane. In particular, we want to understand the implications of this commonly used technique as the membrane system increases in complexity. It is possible that the surface tension used to correct a property such as lipid area per headgroup can have a substantial effect on other lipid properties or on the protein structure.[10,18]

2. Methods

2.1. MD Simulations. We simulated two separate ensembles: (a) NPT for the tension-free state and (b) $NP_z\gamma T$ for the surface tension state. Both ensembles were applied to a peptide-containing system composed of 110 POPC lipids, an alamethicin channel (alm) with four helices, and 3733 water molecules. There were 17 591 total atoms in the system, and the initial size of the simulation box was $6.2 \times 5.5 \times 7.5$ nm^3. The starting configuration of this system is shown in Figure 1. This pre-equilibrated initial structure with an isotropic pressure tensor was obtained from previous extensive studies of the tension-free system.[23,31] The corresponding pure POPC bilayer and water system (128 POPC lipids and 2460 water molecules, 14 036 total atoms, $6.2 \times 6.2 \times 6.9$ nm^3 box) has been discussed in a number of studies.[23,34,35] The four helices of the 20-residue antimicrobial peptide alm were of the form[28] Ac-Aib-Pro-Aib-Ala-Aib-Ala-Gln[7]-Aib-Val-Aib-Gly-Leu-Aib-Pro[14]-Val-Aib-Aib-Glu[18]-Gln-Phl, where Aib is α-aminoisobuteric acid and Phl is phenylalaninol. As discussed by Tieleman,[23] all four Glu[18] side chains were protonated. Alm is an amphiphilic peptide with hydrophilic groups including the alcohol Phl at its C-terminus and hydrophobic groups including acetylated Aib at its N-terminus.[36]

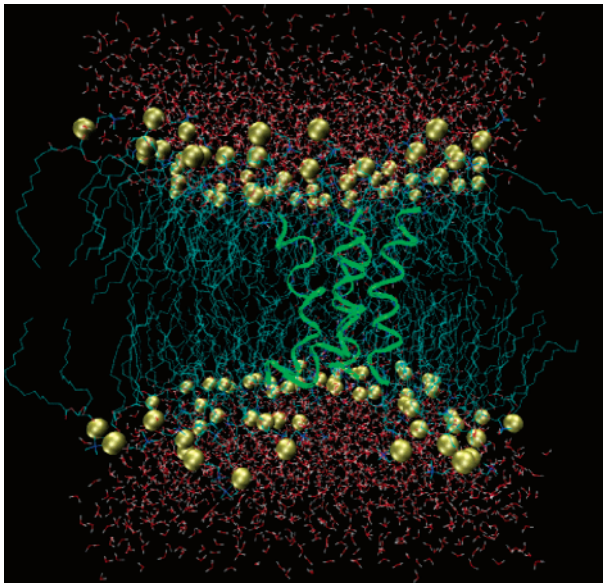

Figure 1. Initial structure of the alm/POPC/water system. Alm helices are represented by green ribbons. POPC phosphate atoms are shown as spheres at their Van der Waals radius, and the lines represent the lipid carbon tails.

2.2. Simulation Details. All simulations were performed using GROMACS 3.2.1.[37,38] The lipid parameters were those described by Berger et al.[24] Alm was described using the modified GROMOS parameter set.[30] Water was modeled using the simple point charge (SPC) model.[39] Two ensembles with periodic boundary conditions were used: NPT and $NP_z\gamma T$.[6,18] The temperature of the lipids, water, and peptide were separately coupled to a 300 K bath using a Berendsen thermostat.[39] This temperature is above the POPC phase transition. For stress-free simulations, an isotropic pressure tensor of 1 bar was applied in NPT and a constant normal pressure, P_z, and a constant surface tension of 1 bar and 20 mN m^{-1} per interface, respectively, were applied in $NP_z\gamma T$. It is now well established that long-range electrostatic interactions are essential to maintain a fluidlike bilayer,[10,15,40] so long-range electrostatic forces were determined using the particle mesh Ewald (PME) method.[12,41] The time step was 2 fs. Bond lengths were constrained by the LINCS algorithm.[42]

Both pure POPC and alm/POPC systems have been studied using MD simulations of tension-free states,[23,31,35] and pre-equilibrated initial states were obtained from Peter Tieleman's website.[43] NPT simulations were initiated directly from these equilibrated systems. For the $NP_z\gamma T$ ensemble, a 1 ns pre-equilibration with a 20 mN m^{-1} surface tension was used to provide a starting configuration for the 10 ns simulations.

It should be noted that the results presented here could have also been obtained from an NP_zAT ensemble, one with a fixed membrane area and a constant normal pressure. This ensemble is useful when the surface area corresponding to the desired surface tension is know a priori or a specific amount of "stretch" is to be applied to the membrane. The surface tension can then be computed as needed.[44] When we refer to properties of the stretched membrane, it should be understood that the same results would be obtained for either ensemble for a given membrane area.

When surface tension is applied to improve the computed lipid properties, the magnitude of the tension depends on factors such as the choice of potential function and treatment of nonbonded interactions.[7] Here, we consider a total surface tension on the system of 40 or 20 mN m^{-1} per interface. This is slightly above the "critical pore-forming" tension for a pure lipid membrane, as determined by Leontiadou et al.[8] Similar values have been obtained from experimental studies that indicate that the critical pore-forming surface tension of of egg PC is 28 ± 4 mN m^{-1}.[45] The value for surface tension used for this simulation is also within the range used to adjust the area per lipid when using other force fields, on pure[6,19] and protein-containing[10] lipid membranes.

Analyses were done using GROMACS analysis tools. The secondary structure analysis of the protein used the Definition of Secondary Structures of Proteins (DSSP) algorithm.[46] Graphical images were obtained using Visual Molecular Dynamics (VMD).[47]

The area per lipid for the protein-containing membrane was determined from the relative solvent-accessible surface area of the lipid headgroups less that of the exposed peptides. This area was computed using SURF[48] as implemented in VMD. The surface area of the lipids was computed from the SURF/VMD images by use of the Digital Image Processing package of Mathematica.[49]

2.3. Statistical Analysis. In our analysis, we are interested in the behavior of relatively small groups of molecules. Because the properties of these groups are not averaged over a large ensemble, there can be considerable variation depending on the initial velocity conditions. Therefore, single run comparisons may not be reliable, even for long-time simulation. So that the effect of surface tension and the protein can be accurately determined, we performed a number of replicate simulations using different random seeds. Normally, six simulations with surface tension and five tension-free simulations were used to compute significance. For the parameters for which confidence limits were determined, all replicates were used. We consider results significant at the 90% level.

Time-dependent parameters often contain considerable thermal noise which makes them appear to have a large variability. Furthermore, we do not know whether short-simulation-time computations result in normally distributed values, particularly when the properties are averaged over too few molecules for the central limit theorem to apply. Therefore, we used robust nonparametric statistical methods. We used two related rank-based methods. For comparing two "treatments" which differed in one factor such as the difference between the mean-square displacement (MSD) in the tension-free membrane and the tensioned membrane, the Mann−Whitney two-sample rank test[50] was used. This test is essentially a nonparametric analogue of the two-sample *t* test and almost as powerful in properly rejecting the null hypothesis: even for normally distributed data, the Mann−Whitney test is 95% as powerful as the *t* test and much more powerful when the assumptions of the *t* test are violated.[50] For comparing more than two factors, the Kruskal−Wallis test[50] was used. This rank-based test is analogous to a single factor ANOVA and is about 95% as powerful.[50]

The Mann−Whitney test was used to determine the significance of differences in hydrogen bonds, the mean-square displacement of lipid phosphate atoms, and membrane areas. The hydrogen bonds at 9 and 10 ns were pooled. This resulted in 22 samples, total, for the NPT and $NP_z\gamma T$ ensembles. For the lipid phosphate mean-square displacement, the lipids were divided into three groups—those with phosphates that were nearest, farthest, and intermediate from the center of the alm bundle. The Kruskal−Wallis test was used to test whether the mobility of lipids differed in these three regions. To compare the tension and tension-free states, all the lipids were pooled and the Mann−Whitney test was used to test the difference between the tension and tension-free states. In each case, the MSD at 10 ns was tested. The Kruskal−Wallis test and the Mann−Whitney test, respectively, were used to investigate whether the lipid order parameter depends on the distance from the alm bundle (by testing the difference in the order parameters of the three lipid regions) and whether the surface tension affected the order parameter. The order parameter investigated was determined with a 10 ns simulation.

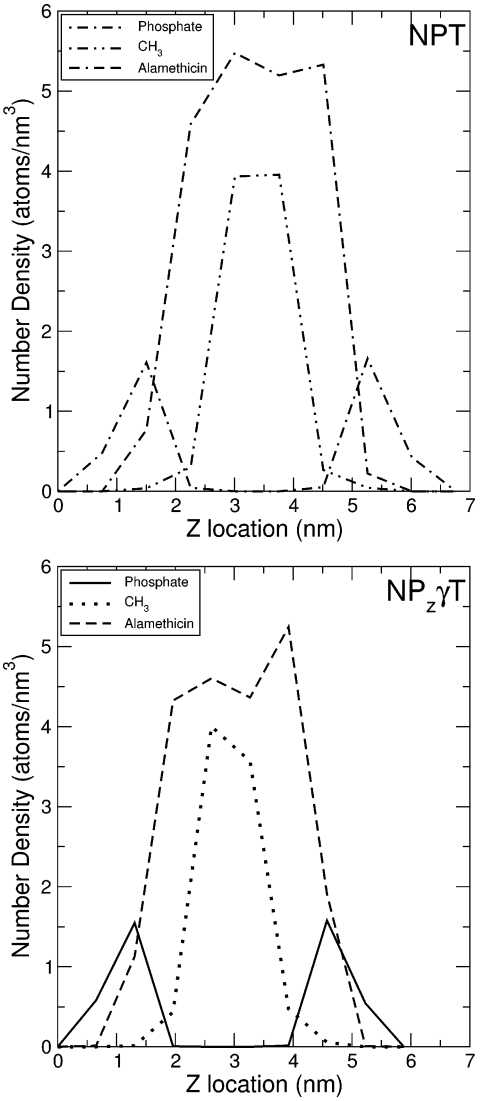

Figure 2. Number density profiles of P and CH_3 for a membrane containing an alm bundle. NPT and $NP_z\gamma T$ simulation ensembles are compared. Densities were averaged over the last 500 ps of the simulations.

Differences in mobility between lipids near and far from the alm bundle within an ensemble were determined by the Wilcoxon paired sample test.[50] This is a rank-based nonparametric equivalent of the paired *t* test that takes into account the magnitude of the difference between the pairs. The mean-square lipid displacements for lipids near and far from the alm were paired by run and time.

For all of the above tests, differences were considered significant at the 90% level, $p < 0.10$.

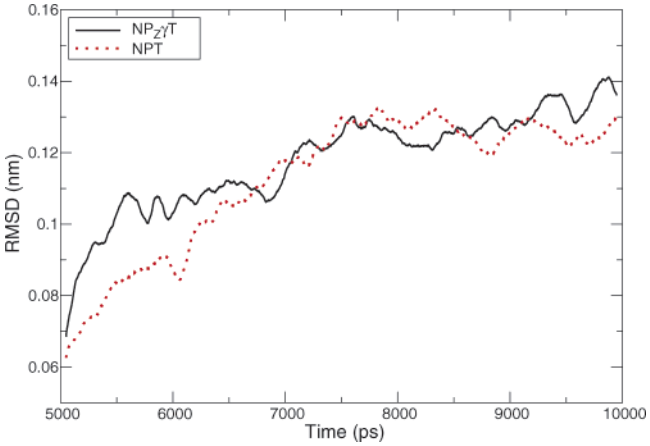

Figure 3. Root-mean-square displacement of a four-helix alm bundle in a POPC membrane. rmsd's were calculated from the backbone atom positions after least-squares fitting on all α-carbon atoms and running averages over 100 ps. The data are the averaged results of five $NP_z\gamma T$ simulations and four NPT simulations using different initial conditions.

3. Results and Discussion

3.1. System Overview. The general structure of the four-peptide alm bundle is shown in Figure 1, which depicts the starting structure of the bundle in the alm/POPC membrane system.

Figure 2 shows the number density distribution profiles of phosphorus atoms, CH_3, and the alm bundle along the normal direction of the membrane surface. The calculations were averages of the last 500 ps of the simulations. The density distributions of NPT runs are quite similar but much different from the results of the $NP_z\gamma T$ run. In the tension state, the membrane interface has thinned to 1.8 nm (determined from phosphate density) which is significant less than that (2.2 nm) in the tension-free state. Because of hydrogen bonding between the lipid and the terminal peptides and because the hydrophobic portion of the peptide corresponds better to the tailgroup region, the alm bundle becomes slightly more compact as the membrane becomes thinner. The width of the density peak of the alm bundle is 4.4 nm in the $NP_z\gamma T$ ensemble compared to 5.1 nm for NPT simulations. The broad CH_3 peaks show significant folding back of the lipid tails, similar to that found by Bachar and Becker.[33] The width of the CH_3 peaks in the tension state (3.7 nm) is smaller than that in the tension-free state (4.3 nm), indicating more order in the lipid tails in the tension state.

3.2. Alm Bundle. *Bundle Stability.* One measure of the conformational stability of the alm bundle on the nanosecond time scale is the root-mean-square deviation (rmsd) of the bundle from the configuration at 5 ns.[31] The average rmsd for the four-helix bundle over the last five nanoseconds of the simulation is shown for both tension and tension-free membranes (Figure 3). Tieleman et al.[31] suggested that the four-helix alm bundle was less stable than bundles containing five, six, or eight helices. They found that the four-helix bundle exhibited greater conformational drift than alm bundles with more helices, or other tetrameric channels. However, in our simulations, the rmsd was considerably lower than that computed by Tieleman et al.[31] This may be the result of a more stable helix packing resulting from an extra 5−7 ns of simulation and the fact that our simulation used the ending alm/lipid configuration of Tieleman et al.[31] as the starting configuration. It should be noted, however, that we use a much different reference structure than that used by Tieleman et al.[31] Root-mean-square fluctuations (rmsf's) (also referred to a 5 ns frame) and the radius of gyration (data not shown) demonstrate similar behavior; there is no difference between the surface tension and tension-free cases.

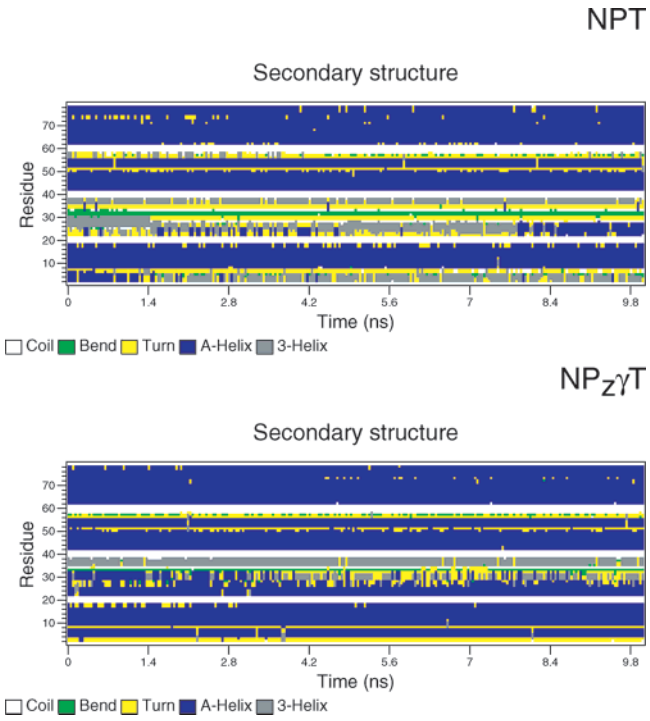

Figure 4. Secondary structure of the alm bundle as a function of time computed by use of the DSSP algorithm.[46] The four-alm peptides are composed of residues 1−21, 22−42, 43−63, and 64−84, respectively. Alm peptides 1 (1−21) and 2 (22−42) show considerably more helical character in the surface tension state.

It is interesting that the distance measures rmsd and rmsf do not differ significantly between the tension-free and surface tension states. Other measures of peptide configuration, such as the number of hydrogen bonds and the secondary structure show significant differences between the two states.

Secondary Structure. The time-dependent secondary structure provides a more detailed description of the conformational stability of the alm bundle in the different simulation ensembles (Figure 4). With surface tension, every helix appears more stable than in the tension-free state, with the greatest difference found in helix 2. For the NPT simulation, alm helix 2 (residues 22−42) loses most of its helical character. For the $NP_z\gamma T$ ensemble, the proportions of bend, turn, and 3_{10} helix are much less than those found for the NPT ensemble. Similar phenomena can be observed by comparing the ending structures of the alm bundle and helix 2 for the NPT and $NP_z\gamma T$ ensembles. Comparison of the bundle structure (Figure 5A) and the structure of helix 2 (Figure 5B) shows differences in the helix structures between the tension and tension-free states consistent with the secondary structure analysis.

Hydrogen Bonding between Alm and POPC. Experimental[51] and computational evidence suggests that hydrogen bonding plays an important role in lipid/water[52] and alm/lipid/water[23,28] interactions. The role of hydrogen bonding in stabilizing the alm bundle as determined from molecular dynamics simulations has been discussed in detail.[23,28] The conclusion was that hydrogen bonding with water dominates but that a number of peptide/lipid hydrogen bonds occur, and they are important for stabilizing the structure. Interactions of the alm bundle with the POPC lipids were examined by measuring the number of hydrogen bonds between the bundle and the lipids as a function of time (Figure 6). If the donor−acceptor distance is $r \le r_{HB} = 0.35$ nm and the donor−acceptor angle is $\alpha \le \alpha_{HB} = 60°$, then

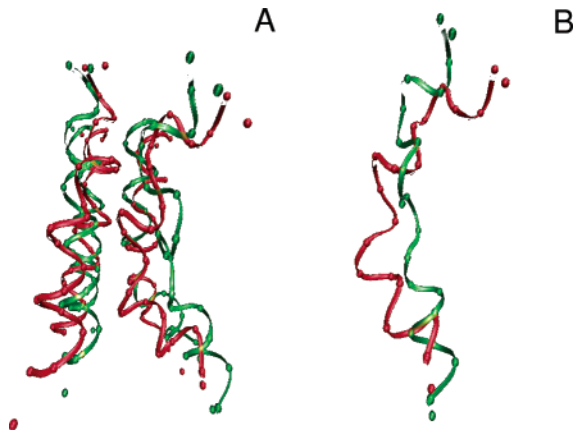

Figure 5. (A) Comparison of the ending structures of the alm bundle between the NP$_z\gamma$T ensemble (red) and the NPT ensemble (green). (B) Comparison of the ending structures of alm helix 2 between the NP$_z\gamma$T ensemble (red) and the NPT ensemble (green). The helices are in ribbon representation, and the spheres in the graphics represent the α-carbon atoms in the helices. The shortening of the bundle in the surface tension thinned membrane enhances its helical character.

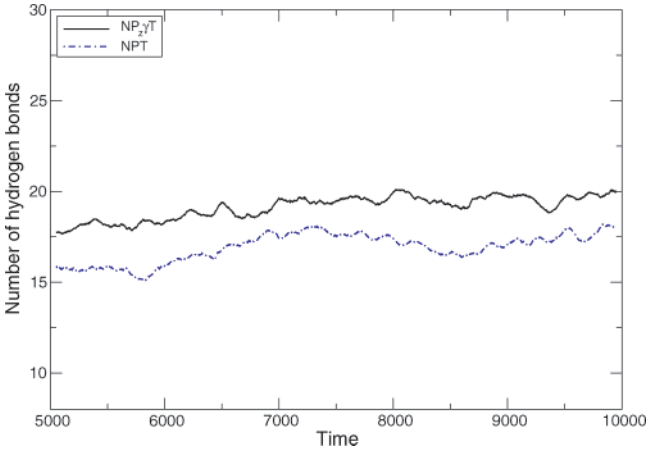

Figure 6. Number of hydrogen bonds between alm and POPC lipids for the NP$_z\gamma$T (solid) and NPT (dashed) ensembles. All of the data are running averages over 100 ps and calculated from the last 5 ns of the 10 ns simulation. Four separate NPT and five separate NP$_z\gamma$T simulations were averaged. The NP$_z\gamma$T simulation includes an extra 1 ns equilibration time. The number of hydrogen bonds formed in the surface tension case is significantly greater than that formed in the tension-free state, $p < 0.1$.

a hydrogen bond is assumed to have been formed.[53] To estimate whether the number of hydrogen bonds was significantly increased by applying surface tension, we used the Mann−Whitney test[50] to compare the total number of computed hydrogen bonds at 9 and 10 ns of simulation, where the number of bonds at these times was pooled. From this analysis, the surface tension state shows significantly more hydrogen bonding, $p < 0.10$. Taken with the increased helicity, as determined from the secondary structure, more hydrogen bonds suggests the conformational stability of the alm bundle increases in the tense state.

Hydrogen bonding of lipid occurs at both the hydrophobic N-terminus and the hydrophilic C-terminus. At the N-terminus end, the Aib[1] peptide nitrogen, the Ala[4] nitrogen, and the Gln[7] nitrogen participate as donors. C-terminus donors include the Glu[18] side-group oxygen, the Gln[19] peptide and side-group nitrogens, and the Phl[20] terminal hydroxyl. The pore formed by the four-helix alm bundle is too narrow for water to readily pass;[28] however, the bundle termini are exposed to the solvent in both the NPT and NP$_z\gamma$T ensembles. As a result, water does penetrate into the pore and interact with a number of residues.

The peptide groups that formed peptide/lipid hydrogen bonds also formed peptide/water hydrogen bonds. Water formed hydrogen bonds with the peptide nitrogens of Ala[6], Aib[10], Val[9], and Val[15]. The number of water/peptide hydrogen bonds did not differ significantly between the NPT and NP$_z\gamma$T ensembles; there were 23.0 ± 2.3 (mean ± SEM, $n = 5$) and 24.4 ± 2.6 ($n = 5$) water hydrogen bonds, respectively (data not shown). Therefore, the number of hydrogen bonds formed between the peptide and the water was not much greater than the number formed between the peptide and the lipid (Figure 6). In simulations of six-helix bundles, which are sufficiently large that the pore is filled with water, Tieleman et al.[23] found a much higher number of water hydrogen bonds per helix than lipid hydrogen bonds per helix. The relatively low number of hydrogen bonds between the water and the peptide is probably the result of the narrow four-helix bundle pore, which restrains both the number of water molecules penetrating and their orientation.

The presence of both water and lipid hydrogen bonding brings up an interesting possibility. In our simulation, the SPC water[39] model was used. While this fixed partial-charge water model gives good bulk properties, polarization effects are included only in a mean-field sense,[54] and such models may improperly describe hydrogen bonding.[55] Had a polarizable water model (see Yu and van Gunsteren[54] for a brief summary and listing of the more popular polarizable water models) been used, it is possible that the increased hydrogen bonding competition from water could reduce the lipid/peptide interaction. If the hydrogen bonding were sufficiently strong to reorient the amino acid side groups, the stability could be reduced. However, the four-alm helix shows about the same number of water hydrogen bonds as lipid hydrogen bonds. Since multiple hydrogen bonds per molecule are common, we would not expect that increased water hydrogen bonding resulting from a polarizable water model would appreciable reduce lipid bonding.

Lopez et al.[52] found that, for water hydrogen bonds with lipids, the probability of forming a bond was dependent on solvent accessibility, and the lifetime of the bond appeared to be affected by competition with other water molecules. For a larger bundle, such as a six-helix bundle, many more water molecules would be in the channel. Their orientational freedom would be greater, and more water hydrogen bonds would form. In this case, it may be possible that increased water hydrogen bond competition would reduce the lipid/protein interaction.

The time-dependent behavior seen in Figure 6 along with that of Figure 3 also suggests that much more time is required for protein/lipid interactions to reach equilibrium than for a pure lipid bilayer under surface tension. About 7 ns is required for the number of hydrogen bonds to stabilize when the alm bundle is in the membrane. Less than 2 ns is sufficient for the pure POPC membrane with surface tension.[10] The additional time required for stabilization is in accord with the relatively slow 5 ns time scale of fluctuations in lipid/protein interactions found by Domene et al.[56]

Figure 7 shows the locations of the atoms that participate in the lipid/peptide hydrogen bonding of Figure 6. The participating peptide residues are discussed above. For lipid hydrogen bonding, the receptors are the carbonyl oxygen in the acyl chains, the glycerol backbone ester bonds with the acyl chains, and the phosphate oxygens. From Figure 7, the effect by which surface tension stabilizes the membrane can be seen clearly. An applied surface tension increases the area per lipid and

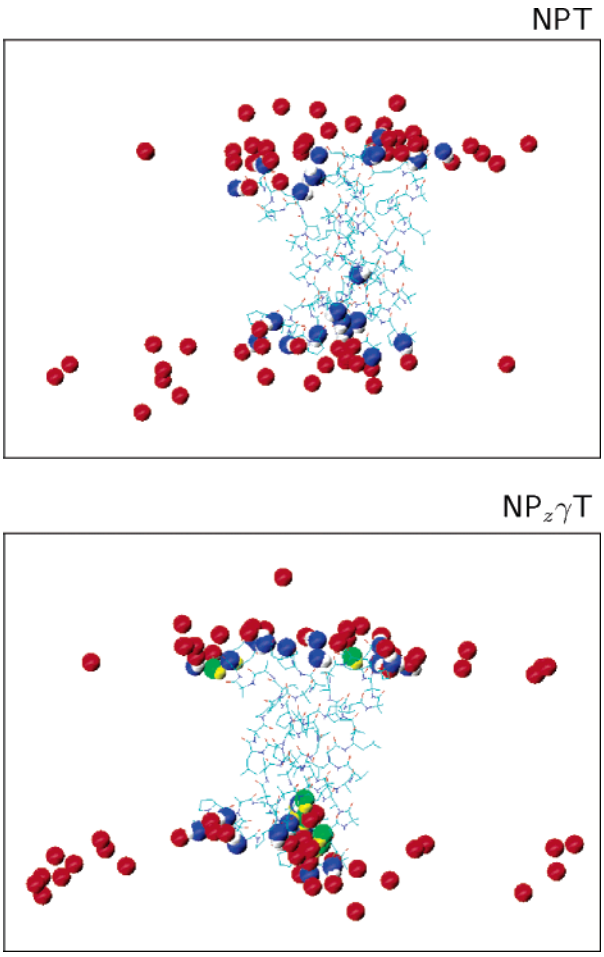

Figure 7. Hydrogen bond donor and acceptors for the alm peptides and POPC lipids. Typical configurations for both the NPT and NP$_z\gamma$T ensembles are shown. Acceptors (red spheres), donors (blue and green spheres), and hydrogens (white and yellow spheres) from five simulations are displayed. The alm is oriented so that the polar C-terminus is up. For any given time, only some of these donors and acceptors are participating. Donors and hydrogens that formed hydrogen bonds in the NP$_z\gamma$T ensemble that did not appear in the NPT ensemble are shown as green and yellow spheres, respectively. Participants from five separate NPT and five separate NP$_z\gamma$T simulations are shown.

reduces the membrane thickness. In reducing the thickness, surface tension reduces the membrane roughness from protrusions and undulations.[7] As a result, the membrane is "pulled down" to the level of the alm termini. The increased helix stability and increased number of hydrogen bonds appear to stem from bringing the lipid hydrogen bond acceptors into the plane of the peptide hydrogen bond donors.

The same lipid groups were hydrogen bond receptors in both the NPT and NP$_z\gamma$T ensembles, although the individual lipids varied with time and run. The lipid acceptors from all five runs are shown in Figure 7; some have diffused away from the bundle. However, the locations of the lipid acceptors give a good measure of the membrane topology in the vicinity of the peptide bundle. Interestingly, the membrane shape strongly conforms to the location of the hydrogen bonds between the lipid and the peptide. This is true for both the hydrophilic (C-terminus, top of bundle) and hydrophobic (N-terminus, bottom of bundle) ends of the peptide bundle.

The two ensembles differed in the residues that acted as hydrogen bond donors, but those differences were confined to the peptide nitrogen backbone. The side-group hydrogen bond participants were the same for either ensemble. Some helix 1

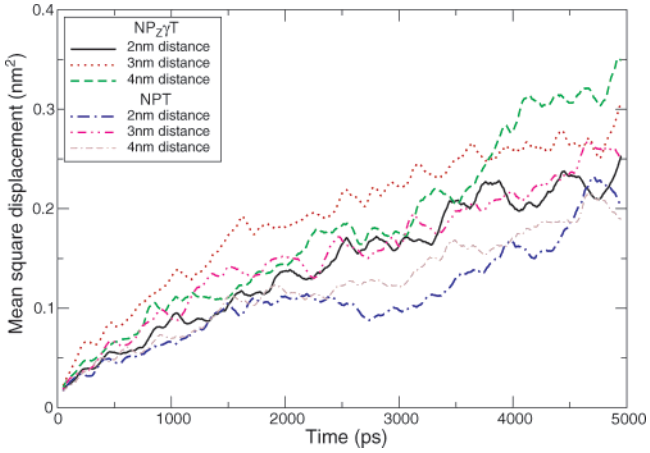

Figure 8. Mean-square displacement (MSD) for the headgroup phosphorus atoms of POPC lipid molecules defined by their distance from the alm bundle. The data represent running averages over 100 ps and calculated from the last 5 ns time period.

hydrogen bonds were lost, but several more were formed in helix 2, the helix that had the largest change in helicity in the NP$_z\gamma$T ensemble (Figure 5).

As might be expected when the membrane is in tension, a somewhat higher proportion of hydrogen bonds form with the phosphate oxygens, since they are more accessible to the alm termini in the thinner membrane. For the NP$_z\gamma$T ensemble, more than 42% of the hydrogen bond acceptors are phosphate oxygens. For the NPT ensemble, fewer than 35% are with phosphate oxygens. Although we did not compute the dynamics of these bonds, previous computations with water at a DMPC lipid bilayer indicate that the double-bonded acyl carbonyl oxygen and the double-bonded phosphate oxygens form hydrogen bonds that have a much longer lifetime than single-bonded oxygens.[52] The thinning of the membrane brings the two phosphate double bond to the level that these oxygens can accept peptide hydrogen bonds.

As indicated in Figure 7, there is a reduction in the thickness of the portion of the membrane that contains the hydrogen bond acceptors: the acyl carbonyl oxygen, the glycerol ester oxygen, and the phosphate oxygen. In addition to the thinning and smoothing effect of surface tension, it is likely that the increased area per lipid of the tension state allows the phosphates room to rotate toward the membrane center, decreasing the distance between the phosphate oxygen and the acyl ester and carbonyl oxygen.

Lipid Mean-Square Displacement. We did not calculate the diffusion coefficients of POPC lipids, since our simulation time scale is not sufficiently long that the computed diffusion constants for lipid lateral diffusion would be valid.[57] Rather, we rely on the nonparametric statistics of several simulations with different initial conditions.

The mobility of the lipids characterized by the lipid mean-square displacement (MSD) is shown in Figure 8. Here, the displacement of a lipid from its initial position is determined by the displacement of the phosphorus atoms on the POPC headgroup in the plane perpendicular to the bilayer normal. Three groups of lipids were chosen to determine if the lipid mobility depends on distance from the alm bundle. The first group was composed of 10 POPC lipids for which the distance of the phosphorus atoms to the alm bundle was 2 ± 0.2 nm (1.8−2.2 nm). The second group included 10 lipids from which the phosphorus atom distance to the alm bundle was 3 ± 0.2 nm (2.8−3.2 nm). The third group included 12 lipids whose

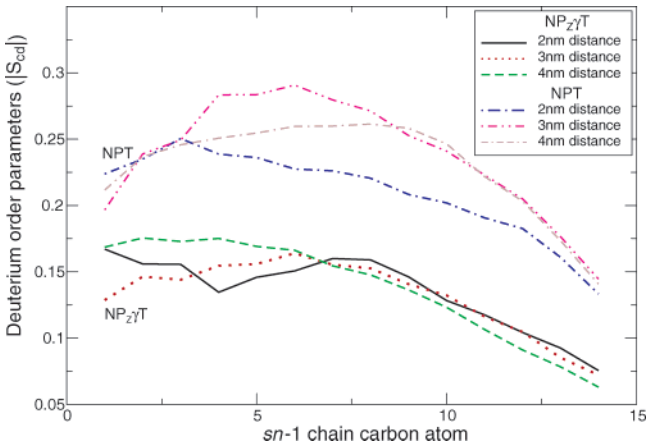

Figure 9. Deuterium order parameters for the *sn*-1 chain of three groups of POPC in the alm/POPC system. The lipid molecules are partitioned according to the distance of the phosphorus atoms from the alm bundle. The order parameter is computed for both the tension and tension-free states.

phosphorus atoms were 4 ± 0.2 nm (3.8−4.2 nm) from the alm bundle. We refer to these groups of lipids as 2, 3, and 4 nm lipids in the following sections.

At the end of the 10 ns simulation, the average MSD value of the phosphorus atoms of all three regions in the five NPT simulations was 0.18 nm^2. The six NP$_z\gamma$T simulations showed a average MSD displacement for the three regions of 0.32 nm^2. The difference between the tension-free membrane and the membrane under surface tension is striking: the MSD of lipids in the membrane under tension is clearly greater than the tension-free membrane, $p < 0.0005$. The large difference in mobility is probably the result of the increased headgroup area per lipid, which increases the diffusional freedom for the lipid molecule.

In addition to the increased mobility of lipids in membranes under tension, the lipid mobility depends on the lipid position relative to the alm bundle. For the NP$_z\gamma$T simulations, the lipids near the alm, 2 ± 0.2, were significantly less mobile than the lipids further from the bundle, $p < 0.025$, although the 2 nm lipids in the surface tension state were still more mobile than the 2 nm lipids in the tension-free state.

It is not surprising that the properties of the lipids which are close to the peptide bundle should be different from those far away from the bundle. The lipids near the alm bundle are strongly influenced by lipid/peptide interactions and short-range forces such as hydrogen bonding. These interactions cause the lipids close to the alm bundle to diffuse more slowly than the "bulk" lipids. As the distance from the lipids to the bundle increases, the mobility of the lipids should also increase. The reduced lipid mobility is likely analogous to the reduced water mobility adjacent to a DMPC membrane, in which the water becomes less mobile from interaction with the lipid by hydrogen bonding. The computations of Lopez et al. show that water associated with lipid oxygen molecules by hydrogen bonding had a diffusion coefficient nearly 100-fold lower than that of free water.[52]

Lipid Order Parameters. The deuterium order parameter (Figure 9) provides a measure of the lipid orientation and therefore can aid in elucidating the effect of surface tension and peptide proximity on that orientation. The deuterium order parameter is defined by

$$S_{CD} = \left\langle \frac{3}{2}\cos^2\theta - \frac{1}{2} \right\rangle$$

where θ is the angle between the CD bond vector and the bilayer normal and the brackets imply averaging over time and molecules.[58] Figure 9 shows the deuterium order parameter of the *sn*-1 chain for both the NPT and NP$_z\gamma$T ensembles.

The carbon tails in the NP$_z\gamma$T ensemble have a lower deuterium order parameter than those in the tension-free state ($p < 0.01$ for 2 nm lipids and $p < 0.0025$ for 3 and 4 nm lipids). This is consistent with the mean-square displacement data which indicates that the phosphorus atoms in the constant surface tension simulation are significantly more mobile than those in the tension-free state. It is also consistent with the increased area per lipid headgroup that would be expected in a system under tension.

Moreover, in the NPT ensemble, the order parameter for lipids 2 nm from the bundle is significantly different than that for POPC lipids farther away (3 and 4 nm) from the bundle ($p < 0.05$ for the *sn*-1 chain and $p < 0.01$ for the *sn*-2 chain). A decreased lipid order parameter near the transmembrane helix bundles has been observed in previous work, as summarized by Tieleman et al.[59] The decreased order appears to be a result of the thicker bilayer of the NPT ensemble enveloping the peptide bundle. In the thicker membrane, the headgroups of the enveloping lipids move between the peptide and the water, but steric hindrance of the peptides requires tails to adapt an increased tilt angle. Figure 7 gives insight into this behavior. Most hydrogen bonds occur at the ester bond oxygen and carbonyl oxygen at the polar end of the lipid acyl tail. Therefore, the hydrogen bond receptors are an indicator of the start of the hydrophobic region. For the thicker NPT membrane (Figure 7, top), the hydrophobic region of the acyl tail is near the size of the peptide and can wrap around the peptide bundle. For the NP$_z\gamma$T ensemble (Figure 7, bottom), the polar part of the fatty acid chain is pulled down to the level of the terminal amino acids. The orientation of the tails of the near lipids is less perturbed by the peptides, since fewer chains wrap over the bundle. The result of membrane thinning is that there is less difference in orientation between lipids near and far from the peptide bundle.

This result is in contrast to MD studies with gramicidin helices that suggested that the hydrocarbon chains of lipids adjacent to the gramicidin had higher order parameter values than those farther away.[20] However, this discrepancy may be a result of the size of the transmembrane bundle. Single helices appear to have less influence on membrane lipids,[59] probably because their smaller size requires less tilt to envelope the bundle. It also differs from the findings of Saiz et al., who used an NPT ensemble to investigate a homopentameric 25-residue α-helical bundle in a dimyristoyl phosphatidylcholine (DMPC) membrane.[26] However, in their system, the peptide was longer, and the lipid tails were shorter, than the system studied here. In their system, it would be unlikely that the lipid would wrap around the bundle.

Interestingly, in the simulations with surface tension, the distance dependence of the order parameter is not seen. The lipids far from the bundle do not have a significantly different order parameter than those close by. Far from the alm bundle, surface tension increases the disorder, because of the additional area per lipid of the stretched membrane. Near the alm bundle, lipid/peptide interactions dominate the lipid behavior, but the lipid/peptide interaction with the polar ends of the acyl tail leaves the rest of the tail free. The net effect of surface tension is therefore to reduce the difference between the order of the near and far lipids. Alternately, one could say that, as the membrane becomes less ordered when stretched under surface tension, the

TABLE 1: Area per Lipid and Solvent-Accessible Area of the Alm Bundle[a]

ensemble	lipid area, Å^2	N-terminus area, Å^2	C-terminus area, Å^2
POPC, est.	64.5		
NP$_z\gamma$T, no peptide	73.0 ± 0.5		
NPT + alm	59.0 ± 0.2	73 ± 7	71 ± 10
NP$_z\gamma$T + alm	70.3 ± 0.6	93 ± 7	137 ± 5

[a] The area per lipid for the peptide-free monolayer is the average estimate from monolayer measurements.[61,62] The difference in area per lipid between the alm-free and alm-containing NP$_z\gamma$T ensembles is significant, $p < 0.05$. The difference in N-terminus solvent-exposed area between the ensembles is not statistically significant.

bundle perturbs the membrane less. Similar order parameter behavior has been seen for membrane/peptide systems as the temperature was increased,[60] which also increases the area per lipid.

Testing the effect of treatment on the order parameter by use of nonparametric statistics is not as well defined as comparing the number of hydrogens or the final MSD. This is because the θ values for adjacent carbon atoms are not independent, and tests of significance assume that the samples are independent. To determine the significance level between two groups of lipids, we computed the significance of each individual CD bond order parameter independently using either the Kruskal−Wallis method (for 2, 3, and 4 nm lipids) or Mann−Whitney method (for tension-free/surface tension). The significance level was determined from the one order parameter that showed the most significant change. For the *sn*-1 chain, this was C8 and C6, respectively, for position or tension comparison, and for the *sn*-2 chain, the corresponding carbons were C11 and C14. This method of computing the confidence interval gives a conservative value, since the true significance should account for the difference in all of the CD bond order parameters, weighted to account for their degree of dependence. This is especially clear for the difference between tension and tension-free states, where all CD bond orders except C1 were significantly lower at $p < 0.05$ to $p < 0.0025$.

Area per Lipid. Because of uncertainty in the contribution of the peptide bundle, the area per lipid is difficult to determine. For a completely embedded protein, the protein volume could be subtracted from the membrane.[25,63] Alm is partially embedded, and the solvent-exposed area increases when surface tension is applied (Table 1). Here, an approximate area per lipid was computed by subtracting the two-dimensional projection of the solvent-accessible peptide area from the solvent-accessible lipid area.

For the NPT ensemble, the area per lipid of the peptide-containing membrane was computed to be 59.0 ± 0.6 Å^2 (SEM, $n = 5$). This is somewhat lower than estimates of 63 or 66 Å^2 based on a POPC monolayer.[61,62]

For peptide-free POPC/water bilayers under a 20 mN m^{-1} surface tension per leaflet with 128 lipids and run parameters the same as the alm-containing membrane, the area per POPC is computed as 73.0 ± 0.5 Å^2 ($n = 3$). The alm-containing membrane had a computed area of slightly, but significantly less, 70.6 ± 0.6 Å^2 (SEM, $n = 6$). Using the Mann−Whitney test as described above, the area per lipid is less in the alm membrane, $p < 0.05$. The area per lipid of the pure POPC membrane is very close to that computed by Gullingsrud and Schulten[17] who used the CHARMM force field. Interpolating their computed values shows that our alm-free area of 73.0 Å^2 per POPC would have been obtained at a surface tension of 22.6 mN m^{-1}. They obtained a monolayer-based experimental estimate of 64 Å^2 with an 11.4 mN m^{-1} surface tension.

Although there is uncertainty in determining the solvent-accessible size of the protein, it is clear that the effect of the alm bundle is to reduce the lipid area. If the area of the peptide were completely ignored (assumed to be 0), the area per lipid in the NP$_z\gamma$T ensemble would be 72.7 ± 0.6 Å^2 ($n = 6$), the same as that of the peptide-free simulation. Therefore, the lipid/peptide interaction must be sufficiently strong to reduce the membrane area to account for the bundle size.

That alm can reduce the lipid area is somewhat surprising, but there is experimental evidence suggesting that is reasonable. Membrane antibacterial peptides have been found to reduce the area per lipid of DMPC membranes at ambient temperature,[60] although in this case the decreased area was associated with increased membrane order and bilayer thickness, which does not occur here. Additionally, the surface pressure−area isotherm for alm/phoshatidylcholine monolayers measured by Ionov et al.[36] shows that vertically inserted alm at alm monolayer surface concentrations corresponding to the bilayer studied here have an average surface area per molecule that is almost independent of alm concentration. Therefore, after subtracting out the area of the alm, the remaining lipid area is essentially constant or perhaps slightly decreasing. Uncertainty in alm orientation (parallel to, or inserted in, the surface) of these data prevents direct comparison with the simulation. However, lipid/peptide hydrogen bonding can apparently perturb the lipid near the peptide bundle (see, e.g., Figure 7). This taken with the strong dependence of the lipid mobility on position (Figure 6) suggests that any reduction in lipid area is local to the vicinity of the peptide.

4. Conclusions

In a previous study, MD simulations of alm bundles containing four to eight helices showed that the four-helix bundle was the least stable.[31] However, applying a constant surface tension to the alm/POPC system increases the conformational stability of the bundle over that in the tension-free state. This is verified by the number of hydrogen bonds between lipid molecules and the alm bundle as determined by the alm secondary structure analysis; with surface tension, the number of hydrogen bonds is more than that in tension-free runs. The increased stability may be explained in terms of the surface tension induced membrane thinning. The hydrogen bond acceptors of the lipid are primarily the ester oxygen bound to the glycerol and the carbonyl oxygen at the polar end of the fatty acid chain. As a result, the surface tension thinned membrane interacts more with the terminal peptide amino acids than the thicker NPT membrane which envelopes the peptide bundle.

It should be mentioned that increasing the bundle stability is not the same as increasing the membrane stability. Indeed, if the lipid/peptide interaction does reduce the lipid area near the helix bundle, as we suggest, increased bundle stability may destabilize the membrane by decreasing the tension required for rupture. With alm in the membrane interacting with nearby lipids, any increase in membrane area is distributed nonuniformly. The membrane in the regions between bundles would be stretched proportionally more, creating instabilities.

We also examined the MSD of lipid phosphorus atoms and the deuterium order parameter as a function of distance from the peptide bundle. In the NP$_z\gamma$T ensemble, we can see the MSD is significantly lower for lipids near the alm bundle, whereas the order parameter is not significantly different at different distances. In the tension-free state, the MSD is independent of position, but the order parameter is different near the alm bundle. A major effect of surface tension in the alm system is that it

significantly increases the MSD of lipids yet significantly reduces the lipid order parameter over the tension-free state. This effect is likely to depend on the type and strength of the lipid/peptide interaction.

The distance measures of peptide structural stability, rmsd and rmsf, do not differ between the tension-free and surface tension states, suggesting that the peptide structure interacts more strongly with its surrounding lipids in the tension state. Since surface tension stretches and thins the membrane, lipids are clearly more mobile and less ordered, yet the peptide fluctuations are unchanged. This reinforces the notion of strong lipid/peptide hydrogen bonding that stabilizes the alm by anchoring it to the nearby lipids.

Implications for General Application of Surface Tension. For our simulation, the degree to which surface tension stretched the membrane was larger than what could be obtained without forming pores in the membrane, Nevertheless, the basic behavior is likely to extend to other $NP_z\gamma T$ or NP_zAT simulations that increase the area of a protein-containing membrane over its equilibrium value.

While applying surface tension does increase the area per lipid, when there is a protein present, the effect on membrane properties is much more complex than just those associated with increased lipid area. At least for alm, altered lipid/peptide interactions of the surface tension thinned membrane cause location-dependent properties. In particular, the lipid membrane does not stretch uniformly because of the peptide/lipid interactions. As a result, lipid mobility and lipid order vary spatially.

Therefore, our results suggest that applying surface tension to a protein-containing membrane may result in spatially dependent property changes. The spatial dependence of the properties will depend on the details of the lipid/peptide interactions as governed by membrane thickness, peptide and lipid chemistry, and the magnitude of the tension. Surprisingly, spatially dependent changes include both properties that become less uniform, as shown by the changes in lipid mobility, and properties that become more uniform, as shown by the order parameters. Therefore, as the complexity of the system increases, caution should be used in applying surface tension solely to attain a given property such as lipid area, rather than based on the physics of the system.

Acknowledgment. Support from National Science Foundation grant 0134594 is gratefully acknowledged.

References and Notes

(1) Singer, S.; Nicolson, G. *Science* **1972**, *175*, 720−731.
(2) Li, C.; Xu, Q. *Cell Signalling* **2000**, *12*, 435−45.
(3) Gooch, K. J., Tennant, C. J., Eds. *Mechanical Forces: Their Effects on Cells and Tissues*; Springer: New York, 1997.
(4) Feller, S. E.; Pastor, R. W. *Biophys. J.* **1996**, *71*, 1350−1355.
(5) Feller, S. E.; Venable, R. M.; Pastor, R. W. *Langmuir* **1997**, *13*, 6555−6561.
(6) Feller, S. E.; Pastor, R. W. *J. Chem. Phys.* **1999**, *111*, 1281−1287.
(7) Marrink, S. J.; Mark, A. E. *J. Phys. Chem. B* **2001**, *105*, 6122−6127.
(8) Leontiadou, H.; Mark, A. E.; Marrink, S. J. *Biophys. J.* **2004**, *86*, 2156−2164.
(9) Feller, S. E.; Zhang, Y.; Pastor, R. W. *J. Chem. Phys.* **1995**, *103*, 10267−10276.
(10) Sankararamakrishnan, R.; Weinstein, H. *J. Phys. Chem. B* **2004**, *108*, 11802−11811.
(11) Brooks, B. R.; Bruccoleri, R. E.; Olafson, B. D.; States, D. J.; Swaminathan, S.; Karplus, M. *J. Comput. Chem.* **1983**, *4*, 183.
(12) Darden, T.; York, D.; Pedersen, L. *J. Chem. Phys.* **1993**, *98*, 10089−10092.
(13) Jahnig, F. *Biophys. J.* **1996**, *71*, 1348−1349.
(14) Lindahl, E.; Edholm, O. *Biophys. J.* **2000**, *79*, 426−433.
(15) Anèzo, C.; de Vries, A. H.; Holtje, H. D.; Tieleman, D. P.; Marrink, S. J. *J. Phys. Chem. B* **2003**, *107*, 9424−9433.
(16) Petrache, H. I.; Zukerman, D. M.; Killian, J. A.; Koeppe, R. E., II; Woolf, T. B. *Langmuir* **2002**, *18*, 1340−1351.
(17) Gullingsrud, J.; Schulten, K. *Biophys. J.* **2004**, *86*, 3496−3509.
(18) Jensen, M. O.; G., M. O.; Peters, G. H. *Biophys. J.* **2004**, *86*, 3556−3575.
(19) Chiu, S. W.; Clark, M.; Balaji, V.; Subramaniam, S.; Scott, H. L.; Jakobsson, E. *Biophys. J.* **1995**, *69*, 1230−1245.
(20) Chiu, S. W.; Subramaniam, S.; Jakobsson, E. *Biophys. J.* **1999**, *76*, 1929−1938.
(21) Róg, T.; Murzyn, K.; Gurbiel, R.; Takaoka, Y.; Kusumi, K.; Pasenkiewicz-Gierula, M. *Biophys. J.* **2001**, *81*, 170−183.
(22) Murzyn, K.; Róg, T.; Jezierski, G.; Takaoka, Y.; Pasenkiewicz-Gierula, M. *J. Lipid Res.* **2004**, *45*, 326−336.
(23) Tieleman, D. P.; Berendsen, H. J. C.; Sansom, M. S. P. *Biophys. J.* **1999**, *76*, 1757−1769.
(24) Berger, O.; Edholm, O.; Jähnig, F. *Biophys. J.* **2000**, *72*, 2002−2013.
(25) Allen, T. W.; Bastug, T.; Kuyucak, S.; Chung, S.-H. *Biophys. J.* **2003**, *84*, 2159−2168.
(26) Saiz, L.; Bandyopadhyay, S.; Klein, M. L. *J. Phys. Chem. B* **2004**, *108*, 2608−2613.
(27) Duclohier, H.; Wroblewski, H. *J. Membr. Biol.* **2001**, *184*, 1−12.
(28) Breed, J.; Biggin, P. C.; Kerr, I. D.; Smart, O. S.; Sansom, M. S. P. *Biochim. Biophys. Acta* **1997**, *1325*, 235−249.
(29) Tieleman, D. P.; Breed, J.; Berendsen, H. J. C.; Sansom, M. S. P. *Faraday Discuss.* **1998**, 209−223.
(30) Tieleman, D. P.; Berendsen, H. J. C.; Sansom, M. S. P. *Biophys. J.* **2001**, *80*, 331−346.
(31) Tieleman, D. P.; Hess, B.; Sansom, M. S. P. *Biophys. J.* **2002**, *83*, 2393−2407.
(32) Woolley, G. A.; Wallace, B. A. *J. Membr. Biol.* **1992**, *129*, 109−136.
(33) Bachar, M.; Becher, O. M. *Biophys. J.* **2000**, *78*, 1359−1375.
(34) Tieleman, D. P.; Sansom, M. S. P.; Berendsen, H. J. C. *Biophys. J.* **1999**, *76*, 40−49.
(35) Tieleman, D. P.; Berendsen, H. J. C.; Sansom, M. S. P. *Biophys. J.* **1999**, *76*, 3186−3191.
(36) Ionov, R.; El-Abed, A.; Angelova, A.; Goldman, M.; Peretti, P. *Biophys. J.* **2000**, *78*, 30026−3035.
(37) Berendsen, H. J. C.; van der Spoel, D.; van Drunen, R. *Comput. Phys. Commun.* **1995**, *95*, 43−56.
(38) Lindahl, E.; Hess, B.; van der Spoel, D. *J. Mol. Model.* **2001**, *7*, 306−317.
(39) Berendsen, H. J. C.; Postma, J. P. M.; van Gunsteren, W. F.; DiNola, A.; Haak, J. R. *J. Chem. Phys.* **1984**, *81*, 3684−3690.
(40) Patra, M.; Karttunen, M.; Hyvnen, M. T.; Falck, E.; Lindqvist, P.; Vattulainen, I. *Biophys. J.* **2003**, *84*, 3636−3645.
(41) Essmann, U.; Perera, L.; Berkowitz, M. L.; Darden, T.; Lee, H.; Pedersen, L. *J. Chem. Phys.* **1995**, *103*, 8577−8593.
(42) Hess, B.; Bekker, H.; Berendsen, H. J. C.; Fraaije, J. G. E. M. *J. Comput. Chem.* **1997**, *18*, 1463−1472.
(43) Tieleman, D. P. http://moose.bio.ucalgary.ca. (accessed Sept 2005).
(44) Zhang, Y.; Feller, S. E.; Brooks, B. R.; Pastor, R. W. *J. Chem. Phys.* **1995**, *103*, 10252−10266.
(45) Hull, M. C.; Sauer, D. B.; Hovis, J. S. E. *J. Phys. Chem. B* **2004**, *108*, 15890−15895.
(46) Kabsch, W.; Sander, C. *Biopolymers* **1983**, *22*, 2577−2637.
(47) Humphrey, W.; Dalke, A.; Schulten, K. *J. Mol. Graphics* **1996**, *14*, 33−38.
(48) Varshney, A.; Brooks, F. P.; Wright, W. V. *IEEE Comput. Graphics Appl.* **1994**, *14*, 19−25.
(49) *Mathematica*, version 5.1; Wolfram Research, Inc.: Champaign, IL, 2004.
(50) Zar, J. H. *Biostatistical Analysis*, 4th ed.; Prentice Hall: Upper Saddle River, NJ, 1999.
(51) Ionov, R.; El-Abed, A.; Goldmann, M.; Peretti, M. *J. Phys. Chem. B* **2004**, *108*, 8485−8488.
(52) Lopez, C. F.; Nielsen, S. O.; Klein, M. L.; Moore, P. B. *J. Phys. Chem. B* **2004**, *108*, 6603−6610.
(53) van der Spoel, D.; van Buuren, A. R.; Apol, E.; Meulenhoff, P. J.; Tieleman, D. P.; Sijbers, A. L. T. M.; Hess, B.; Feenstra, K. A.; Lindahl, E.; van Drunen, R.; Berendsen, H. J. C. *Gromacs User Manual*, version 3.0; 2001. FTP site: ftp://ftp.gromacs.org/pub/manual-3.2.pdf (accessed Sept 2005).
(54) Yu, H.; van Gunsteren, W. F. *J. Chem. Phys.* **2004**, *121*, 9549−9564.
(55) Stillinger, F. H. *Science* **1980**, *209*, 451−457.
(56) Domene, C.; Bond, P. J.; Deol, S. S.; Samson, M. S. P. *J. Am. Chem. Soc.* **2003**, *125*, 14966.
(57) Blume, A. Dynamic Properties. In *Phospholipids Handbook*; Cevc, G., Ed.; Marcel Dekker: New York, 1993.

(58) Leach, A. R. *Molecular Modelling*; Longman: Singapore, 1996.
(59) Tieleman, D. P.; Forrest, L. R.; Sansom, M. S. P.; Berendsen, H. J. C. *Biochemistry* **1998**, *37*, 17554−17561.
(60) Henzler-Wildman, K. A.; Martinez, G. V.; Brown, M. F.; Ramamoorthy, A. *Biochemistry* **2004**, *43*, 8459−8469.
(61) Smaby, J. M.; Momsen, M. M.; Brockman, H. L.; Brown, R. M. *Biophys. J.* **1997**, *73*, 1492−1505.
(62) Hyslop, P. A.; Morel, B.; Sauerheber, R. D. *Biochemistry* **1990**, *29*, 1025−1038.
(63) Wolf, T. B.; Roux, B. *Proteins* **1996**, *24*, 92−114.